

Article

# Assessing the Performance of the WOFOST Model in Simulating Jujube Fruit Tree Growth under Different Irrigation Regimes

Tiecheng Bai <sup>1,2</sup>, Nannan Zhang <sup>1</sup>, Youqi Chen <sup>3,\*</sup> and Benoit Mercatoris <sup>2,\*</sup> 

<sup>1</sup> College of Information Engineering, Tarim University, Akaer 843300, China; baitiecheng@taru.edu.cn (T.B.); zhangnannan@taru.edu.cn (N.Z.)

<sup>2</sup> TERRA Teaching and Research Centre, Gembloux Agro-Bio Tech, Liège University, Passage des Déportés, 2, 5030 Gembloux, Belgium

<sup>3</sup> Institute of Agricultural Resources and Regional Planning of CAAS, No. 12 Zhongguancun South St., Haidian District, Beijing 100081, China

\* Correspondence: chenyouqi@caas.cn (Y.C.); benoit.mercatoris@uliege.be (B.M.)

Received: 12 February 2019; Accepted: 5 March 2019; Published: 9 March 2019



**Abstract:** Cropping system models are widely employed to evaluate plant water requirements and growth situations. However, these models rarely focus on growth studies of perennial fruit trees. The aim of this study was to evaluate the performance of the WOFOST (WORld FOod STudies) model in simulating jujube fruit tree growth under different irrigation treatments. The model was calibrated on data obtained from full irrigation treatments in 2016 and 2017. The model was validated on four deficit percentages (60%, 70%, 80%, and 90%) and one full irrigation treatment from 2016 to 2018. Calibrated  $R^2$  and RMSE values of simulated versus measured soil moisture content, excluding samples on the day of irrigation and first day after irrigation, reached 0.94 and  $0.005 \text{ cm}^3 \text{ cm}^{-3}$ . The model reproduced growth dynamics of the total biomass and leaf area index, with a validated  $R^2 = 0.967$  and  $\text{RMSE} = 0.915 \text{ t ha}^{-1}$ , and  $R^2 = 0.962$  and  $\text{RMSE} = 0.160 \text{ m}^2 \text{ m}^{-2}$ , respectively. The model also showed good global performance, with  $R^2 = 0.86$  and  $\text{RMSE} = 0.51 \text{ t ha}^{-1}$ , as well as good local agreement ( $R^2 \geq 0.8$ ) and prediction accuracy ( $\text{RMSE} \leq 0.62 \text{ t ha}^{-1}$ ) for each growth season. Furthermore, 90% of full irrigation can be recommended to achieve a balance between jujube yields and water savings (average decline ratio of yield  $\leq 3.8\%$ ).

**Keywords:** jujube fruit; crop growth model; soil water balance; irrigation degree; growth simulation

## 1. Introduction

Jujube (*Zizyphus jujuba* Miller) fruit is rich in vitamin C, amino acids, carbohydrates, and minerals, and has been widely used in traditional foods, food additives, flavorings, and raw materials in traditional Chinese medicine [1], as well as medicinal supplements [2]. Jujube trees are widely cultivated in the subtropical and tropical regions of Asia, with approximately 3.25 million hectares in China. The southern region of Xinjiang Uygur Autonomous Region has the highest output, of about 3.26 million tons, and supplies high quality jujube because of the large temperature difference and sufficient light in this region. However, in this arid and warm-temperate region, average annual rainfall ranges from 77 mm to 106 mm, and crop growth highly depends on irrigation. How to use water resources effectively and how to implement precision agricultural irrigation are particularly important for this water-deficient area, which are also important parts of sustainable agricultural production.

Crop growth models derived from mathematical descriptions have become more advanced. They are widely applied in agricultural production management and societally relevant applications such

as climate change responses [3–8], crop yield predictions [9–13], and understanding crop responses in field experimentation and the environment [14–16]. New applications for precision agriculture are also expected with the development and improvement of such models [17]. Over the past decades, crop models have been developed, and the prominent models are WOFOST (WORld FOod STudies) [18], DSSAT (Decision Support System for Agrotechnology Transfer) [19], EPIC (Environmental Policy Integrated Climate) [20], STICS (Multidisciplinary simulator for standard crops) [21] and APSIM (Agricultural Production Systems sIMulator) [22]. In addition, other models, such as SWAP (Soil, Water, Atmosphere and Plant) [23], AquaCrop (Crop-water productivity model) [24] and CropSyst (Cropping Systems Simulation Model) [25], are constantly being added for different crops and purposes.

The core of any crop growth model is that a set of equations are employed to estimate biomass production from the captured carbon dioxide, solar radiation, and water, mainly including carbon-driven (WOFOST), radiation-driven (EPIC and STICS), and water-driven (CropSyst and AquaCrop) models [15]. Although the driving mechanism of several models is different, many models can be used to perform growth simulations under water stress conditions by considering water balance components, thereby accomplishing crop growth simulation and yield prediction [26–30], as well as evaluating crop water requirements and implementing irrigation management [31–35]. In addition, the water-driven AquaCrop model has been successfully employed to optimize fertigation strategies for orange production, predict the yield of peach trees under different deficit percentages [36,37], and evaluate the transpiration reductions of mature olive trees [38]. Scheduling regulated deficit irrigation in a pear orchard is also implemented by the CropSyst model [39]. Certainly, calibration and validation should be taken into account according to crop varieties, irrigation systems, and meteorological environments [16,40,41] in the case of specific applications.

The WOFOST model has also been widely applied in the water-limited growth simulation of annual crops by creating a soil water balance model that responds to the change of soil moisture content [17], such as cotton, maize, winter wheat, rice, and sugar beet. However, few studies have focused on using the WOFOST model to simulate the growth of fruit trees. The reason may be that tree ages and tree shapes vary greatly in different planting areas, thereby resulting in initial total dry weight and carbon dioxide assimilation parameters that are not easily determined. Whether the WOFOST model can be employed for the growth simulation of perennial fruit trees presents a valuable research objective, which may expand on the application of crop growth models in fruit tree production. The aim of this study was to assess the performance of the WOFOST model in reproducing jujube growth under different deficient irrigation treatments. Furthermore, simulated growth dynamics of above-ground total biomass, leaf area index, soil moisture content, and harvestable yield were evaluated and discussed based on detailed field experimental data from 2016 to 2018.

## 2. Materials and Methods

### 2.1. Site and Climate of Experimental Field

The experiments were conducted at two jujube orchards during the growing seasons of 2016, 2017, and 2018 in Alar, Southern Xinjiang (E 81°13', N 40°35'). Jujube trees were planted in 2009 in a sandy loam soil around 1–1.2 m deep over bedrock. The experimental fields were characterized by a typical arid warm-temperate region, with a total annual rainfall of 106 mm, 98 mm, and 77 mm in 2016, 2017, and 2018, respectively, distributed mostly during summer. An average photoperiod was about 15 hours from April to October, and average annual temperature ranged from 10.8 °C to 12.5 °C, with a maximum daily temperature difference of 20 °C. Due to the excellent light and heat resources, the quality of jujube fruit was higher in the region than others.

Climate data, including daily values of wind speed, solar radiation, photosynthetically active radiation (PAR), air temperature, humidity, and precipitation, were measured at an automatic weather station of the Alar Agricultural Irrigation Station, located about 500 meters away from the experimental fields.

## 2.2. Experimental Treatments

Jujube fruit trees (cultivar, *jun jujube*) were characterized by high quality fruit, high yields, and drought resistance with about 6165 plants per hectare. During each jujube growing season (2016 to 2018), the fertilization amounts of converted pure nitrogen (N), phosphorus pentoxide ( $P_2O_5$ ), and potassium oxide ( $K_2O$ ) were 375, 240, and 300  $kg\ ha^{-1}$ , respectively. A first pour of the fertilizer was spread by drip irrigation during the emergence and flowering periods (N: 50%,  $P_2O_5$ : 80%, and  $K_2O$ : 70%), and the rest of the fertilizer was fertilized in the fruit growth period (N: 50%,  $P_2O_5$ : 20%, and  $K_2O$ : 30%). Pests and diseases were effectively controlled through standard management.

Irrigation experiments, with three replicates, included five treatments: full irrigation (375 mm, D1), 90% of full irrigation supply (338 mm, D2), 80% (300 mm, D3), 70% (263 mm, D4), and 60% (225 mm, D5). The full irrigation amount referred to an empirical value that was determined using an spreadsheet irrigation management tool [42], which employed meteorological, soil, and jujube parameters to evaluate water requirements. The 375 mm value was an empirical irrigation value commonly used in the local area in prior years, which can be assumed to be rich in jujube fruit growth during the main development period. Irrigation was carried out in ten portions during the emergence, flowering, and fruit development periods. During the early emergence period, water and other nutrients were thoroughly supplied to make sure there was normal emergence.

A small canopy permanent line tree shape was implemented in all field experimental plots to avoid the effect of tree shape on the simulation results.

## 2.3. Data Measurement and Collection

Phenological development stages, including the emergence date, end date of flowering, and maturity, were observed from 2016 to 2018.

According to the requirements of the WOFOST model, the biomass indicators to be measured mainly included the initial total crop dry weight (TDWI), above-ground biomass, and leaf area index. Jujube trees differed from annual crops, and if the stems of the previous year were considered, they could lead to exaggerated TDWI values. In this research, TDWI at emergence was redefined as the weight of the initial new organs (initial buds and roots), which was calculated by measuring the weight of buds and roots. Leaf area index (LAI) and total above-ground biomass (TAGP, living leaves, stems, and storage organ weight) during the growth period were measured approximately ten times at each plot. At each test, ten trees were selected, and one-quarter of the stems, leaves, and fruits of each tree was brought back to the laboratory, dried to a constant weight, and weighed. The yield of the sampled loss was finally added to the final yield at each point (almost 411 trees per spot). LAI and extinction coefficient for diffuse visible light were measured by using a fruit tree canopy analyzer (TOP-1300, Zhejiang Top Cloud-agri Technology CO., LTD., Hangzhou, China, Figure 1a), which was corrected by standard measurement methods. The depth and weight of the root were sampled and measured by digging a 90-degree profile (Figure 1b).  $CO_2$  assimilation parameters including light-use efficiency, single leaf and maximum leaf  $CO_2$  assimilation rate were obtained by fitted light response curves based on net photosynthetic rate data measured using an LI-COR 6400XT meter.

The soil physical properties, including average volumetric water content at field capacity ( $0.194\ cm^3\ cm^{-3}$ ), saturated soil moisture content ( $0.39\ cm^3\ cm^{-3}$ ), average bulk density ( $1.523\ g\ cm^{-3}$ ), hydraulic conductivity, and water retention curves, were measured before emergence each year. The soil moisture content at different depths was automatically monitored with two-hour intervals by the corrected soil moisture automatic monitoring meters (HOBO H21-002, United States) that were installed at 0, 20, 40, 60, and 80 cm, respectively.



**Figure 1.** (a) Leaf area index (LAI) and canopy parameter measurement; (b) Depth and weight of roots measurement.

The jujube yield data for five irrigation gradients from 2016 to 2018 are shown in Table 1, with standard deviations ranging from 0.866 to 1.14 t ha<sup>-1</sup>, which was beneficial for model evaluation. The highest average yield occurred in 2017, then 2018, and finally 2016.

**Table 1.** Yield data for three years.

Year	Yield for Different Irrigation Degree (t ha <sup>-1</sup> )						SD
	D1	D2	D3	D4	D5	Average	
2016	6.380	5.733	6.149	4.716	4.115	6.380	0.866
2017	9.155	8.738	7.490	7.398	5.918	9.155	1.140
2018	7.767	6.981	7.259	5.409	5.039	7.767	1.071

D1: full irrigation; D2: 90% of full irrigation supply; D3: 80% of full irrigation; D4: 70% of full irrigation; D5: 60% of full irrigation, SD: Standard Deviation.

#### 2.4. Model Calibration and Validation Process

Jujube parameters were calibrated for the full irrigation treatment with the data from 2016 and 2017 according to the principle of average correlation and error minimization, and the results in 2018 were used to validate TAGP and LAI growth dynamics. The soil water balance module was calibrated for the full irrigation treatment in 2017 based on daily monitoring data of soil moisture content.

The calibration process of the WOFOST model was suggested in De Wit and Wolf [43]. First, the length of the growth period and phenology would be effectively simulated for a reliable biomass and yield prediction, which was determined by the effective accumulated temperature method [18]. TSUMEM (temperature sum from sowing to emergence), TSUM1 (temperature sum from emergence to flowering), and TSUM2 (temperature sum from flowering to maturity) were calibrated by daily average temperature and emergence, flowering, and maturity date from years 2016 and 2017. Second, light interception and potential biomass production were mainly determined by leaf-related and CO<sub>2</sub> assimilation parameters. Specific leaf area (SLATB), LAI at emergence (LAIEM), and a maximum relative increase in LAI (RGR<sub>LAI</sub>) were calibrated by the measured TAGP and LAI results, and CO<sub>2</sub> assimilation parameters were calculated with photosynthesis light-response curves. Concurrently, the assimilation distribution between crop organs was determined in dependence of the crop development stages and elaboration of experimental biomass data. Finally, the degree of drought stress and the resulting reductions in transpiration rate and photosynthesis were determined by the soil moisture content in the root zone and the water stress correction factor [15].

The model evaluations were based on the comparison between simulated and observed data for all treatments in three years. The agreement between measured and simulated yield was quantified using a coefficient of determination ( $R^2$ ). The root mean square error (RMSE), the mean absolute error (MAE), and the mean bias error (MBE) were used to evaluate prediction accuracy.  $R^2$  can give the percentage of samples that can be interpreted by the model to all samples. The RMSE can show a weighted change in the error (residual) between the predicted and actual values. MAE and MBE were mainly used to further analyze the simulation performance for different years. MAE can give the most intuitive and clear indicator for the average yield error magnitude. MBE can be used to evaluate whether the model overestimated or underestimated actual yield and can also express the uniformity of the error distribution.

Values were calculated by the following equations:

$$R^2 = 1 - \frac{\sum_{i=1}^n (y_i - \tilde{y}_i)^2}{\sum_{i=1}^n (y_i - \bar{y}_i)^2} \quad (1)$$

$$\text{RMSE} = \sqrt{\frac{\sum_{i=1}^n (\tilde{y}_i - y_i)^2}{n}} \quad (2)$$

$$\text{MAE} = \sum_{i=1}^n |y_i - \tilde{y}_i| \quad (3)$$

$$\text{MBE} = \sum_{i=1}^n (y_i - \tilde{y}_i) \quad (4)$$

where  $\tilde{y}_i$  was the simulated value based on the model,  $y_i$  was the measured value,  $\bar{y}_i$  was the mean of the measured values, and  $n$  was the number of samples.

### 3. Results and Discussion

#### 3.1. Model Calibration and Validation under Full Irrigation

The calibrated jujube parameters are presented in Table 2. These parameters were obtained in the following ways: with measured data, with estimated values from the available information and observed data, from calibrated values based on field-measured data, and from default average values or fine-tuning values around default data.

**Table 2.** Calibrated model parameters.

Parameter	Description	Value	Units	Source
<b>*Emergence</b>				
TBASEM	lower threshold temperature emergence	10	°C	e
TEFFMX	max effective temperature emergence	30	°C	e
TSUMEM	temperature sum from sowing to emergence	230	°C	m-c
<b>*Phenology parameter</b>				
TSUM1	temperature sum from emergence to anthesis	967	°C d <sup>-1</sup>	m-c
TSUM2	temperature sum from anthesis to maturity	960	°C d <sup>-1</sup>	m-c
DTSMTB0	daily increase in temperature sum as a function of average at = 0 °C	0.00	°C d <sup>-1</sup>	e
DTSMTB100	daily increase in temperature sum as a function of average at = 10 °C	0	°C d <sup>-1</sup>	e
DTSMTB355	daily increase in temperature sum as a function of average at = 35.5 °C	25.5	°C d <sup>-1</sup>	e
DTSMTB400	daily increase in temperature sum as a function of average at = 40 °C	25.5	°C d <sup>-1</sup>	e

Table 2. Cont.

Parameter	Description	Value	Units	Source
<b>*Initial parameters</b>				
TDWI	Redefine initial total emergence dry weight	15.1/17.2/19.4	kg ha <sup>-1</sup>	m
LAIEM	leaf area index at emergence	0.0007	ha ha <sup>-1</sup>	d
RGRLAI	maximum relative increase in LAI	0.05	ha ha <sup>-1</sup> d <sup>-1</sup>	d
<b>*Green area</b>				
SLATB000	specific leaf area when DVS = 0	0.00165	ha kg <sup>-1</sup>	m-c
SLATB55	specific leaf area when DVS = 0.55	0.0013	ha kg <sup>-1</sup>	m-c
SLATB100	specific leaf area when DVS = 1	0.0013	ha kg <sup>-1</sup>	m-c
SLATB200	specific leaf area when DVS = 2	0.0014	ha kg <sup>-1</sup>	m-c
SPAN	life span of leaves growing at 35 degrees Celsius	60	[d]	e
TBASE	lower threshold temp. for ageing of leaves	10	°C	e
<b>*CO<sub>2</sub> assimilation</b>				
KDIFTB00	extinction coefficient for diffuse visible light at DVS = 0	0.8	\	m-c
KDIFTB200	extinction coefficient for diffuse visible light at DVS = 2	0.8	\	m-c
EFFTB19.5	light-use efficiency single leaf at average temp. = Celsius	0.495	kg ha <sup>-1</sup> hr <sup>-1</sup> J <sup>-1</sup> m <sup>2</sup> s	m-c
EFFTB355	light-use efficiency single leaf at average temp. = Celsius	0.495	kg ha <sup>-1</sup> hr <sup>-1</sup> J <sup>-1</sup> m <sup>2</sup> s	m-c
AMAXTB00	maximum leaf CO <sub>2</sub> assimilation. Rate at DVS = 0	39.0	kg ha <sup>-1</sup> hr <sup>-1</sup>	m-c
AMAXTB170	maximum leaf CO <sub>2</sub> assimilation. Rate at DVS = 1.7	39.0	kg ha <sup>-1</sup> hr <sup>-1</sup>	m-c
AMAXTB200	maximum leaf CO <sub>2</sub> assimilation. Rate at DVS = 2	20.0	kg ha <sup>-1</sup> hr <sup>-1</sup>	m-c
TMPFTB10	reduction factor of AMAX at 10 °C	0	\	d
TMPFTB195	reduction factor of AMAX at 19.5 °C	1	\	d
TMPFTB355	reduction factor of AMAX at 35.5 °C	1	\	d
<b>*Conversion of assimilates into biomass</b>				
CVL	efficiency of conversion into leaves	0.732	kg kg <sup>-1</sup>	m-c
CVO	efficiency of conversion into storage organs	0.780	kg kg <sup>-1</sup>	m-c
CVR	efficiency of conversion into roots	0.690	kg kg <sup>-1</sup>	m-c
CVS	efficiency of conversion into stems	0.751	kg kg <sup>-1</sup>	m-c
<b>* maintenance respiration</b>				
Q10	Relative increase in respiration rate per 10 °C temperature increase	2	kg CH <sub>2</sub> O kg <sup>-1</sup> d <sup>-1</sup>	d
RML	Relative maintenance respiration rate of leaves	0.03	kg CH <sub>2</sub> O kg <sup>-1</sup> d <sup>-1</sup>	d
RMO	Relative maintenance respiration rate of storage organs	0.01	kg CH <sub>2</sub> O kg <sup>-1</sup> d <sup>-1</sup>	d-c
RMR	Relative maintenance respiration rate of roots	0.01	kg CH <sub>2</sub> O kg <sup>-1</sup> d <sup>-1</sup>	d
RMS	Relative maintenance respiration rate of stems	0.015	kg CH <sub>2</sub> O kg <sup>-1</sup> d <sup>-1</sup>	d-c
<b>*Dartitioning parameters</b>				
FRTB00	fraction of above-ground dry matter to roots at DVS = 0	0.3	kg kg <sup>-1</sup>	m-c
FRTB154	fraction of above-ground dry matter to roots at DVS = 1.54	0.0	kg kg <sup>-1</sup>	m-c
FLTB00	fraction of above-ground dry matter to leaves at DVS = 0	0.67	kg kg <sup>-1</sup>	m-c
FLTB012	fraction of above-ground dry matter to leaves at DVS = 0.12	0.31	kg kg <sup>-1</sup>	m-c
FLTB022	fraction of above-ground dry matter to leaves at DVS = 0.22	0.41	kg kg <sup>-1</sup>	m-c
FLTB032	fraction of above-ground dry matter to leaves at DVS = 0.32	0.55	kg kg <sup>-1</sup>	m-c
FLTB051	fraction of above-ground dry matter to leaves at DVS = 0.51	0.4	kg kg <sup>-1</sup>	m-c
FLTB097	fraction of above-ground dry matter to leaves at DVS = 0.97	0.15	kg kg <sup>-1</sup>	m-c
FLTB100	fraction of above-ground dry matter to leaves at DVS = 1.00	0.1	kg kg <sup>-1</sup>	m-c
FLTB145	fraction of above-ground dry matter to leaves at DVS = 1.45	0	kg kg <sup>-1</sup>	m-c
FLTB200	fraction of above-ground dry matter to leaves at DVS = 2.00	0	kg kg <sup>-1</sup>	m-c
FSTB00	fraction of above-ground dry matter to stems at DVS = 0	0.33	kg kg <sup>-1</sup>	m-c
FSTB012	fraction of above-ground dry matter to stems at DVS = 0.12	0.69	kg kg <sup>-1</sup>	m-c
FSTB022	fraction of above-ground dry matter to stems at DVS = 0.22	0.59	kg kg <sup>-1</sup>	m-c
FSTB032	fraction of above-ground dry matter to stems at DVS = 0.32	0.45	kg kg <sup>-1</sup>	m-c
FSTB051	fraction of above-ground dry matter to stems at DVS = 0.51	0.6	kg kg <sup>-1</sup>	m-c
FSTB097	fraction of above-ground dry matter to stems at DVS = 0.97	0.85	kg kg <sup>-1</sup>	m-c
FSTB100	fraction of above-ground dry matter to stems at DVS = 1.00	0.43	kg kg <sup>-1</sup>	m-c
FSTB145	fraction of above-ground dry matter to stems at DVS = 1.45	0.2	kg kg <sup>-1</sup>	m-c
FSTB200	fraction of above-ground dry matter to stems at DVS = 2.00	0	kg kg <sup>-1</sup>	m-c
FOTB00	fraction of above-ground dry matter to storage organs at DVS = 0	0	kg kg <sup>-1</sup>	m-c
FOTB012	fraction of above-ground dry matter to storage organs at DVS = 0.12	0	kg kg <sup>-1</sup>	m-c
FOTB022	fraction of above-ground dry matter to storage organs at DVS = 0.22	0	kg kg <sup>-1</sup>	m-c
FOTB032	fraction of above-ground dry matter to storage organs at DVS = 0.32	0	kg kg <sup>-1</sup>	m-c
FOTB051	fraction of above-ground dry matter to storage organs at DVS = 0.51	0	kg kg <sup>-1</sup>	m-c

Table 2. Cont.

Parameter	Description	Value	Units	Source
FOTB097	fraction of above-ground dry matter to storage organs at DVS = 0.97	0	kg kg <sup>-1</sup>	m-c
FOTB100	fraction of above-ground dry matter to storage organs at DVS = 1.00	0.47	kg kg <sup>-1</sup>	m-c
FOTB145	fraction of above-ground dry matter to storage organs at DVS = 1.45	0.8	kg kg <sup>-1</sup>	m-c
FOTB164	fraction of above-ground dry matter to storage organs at DVS = 1.64	1.0	kg kg <sup>-1</sup>	m-c
FOTB200	fraction of above-ground dry matter to storage organs at DVS = 2.00	1	kg kg <sup>-1</sup>	m-c
<b>*Death rates</b>				
RDRSTB00	Relative death rate of stems at DVS = 0	0	\	e
RDRSTB200	Relative death rate of stems at DVS = 2.0	0	\	e
<b>Water use and soil parameters</b>				
CFET	correction factor transpiration rate	1.02	-	d-c
DEPNR	correction factor for crop water stress sensitivity	1.5	-	c
RDI	initial rooting depth	10	cm	d
RRI	maximum daily increase in rooting depth	1.2	cm d <sup>-1</sup>	e
RDMCR	maximum rooting depth	120	cm	m
SMW	soil moisture content at wilting point	0.0449	cm <sup>3</sup> cm <sup>-3</sup>	e
SMFCF	soil moisture content at field capacity	0.198	cm <sup>3</sup> cm <sup>-3</sup>	m-c
SM0	soil moisture content at saturation	0.39	cm <sup>3</sup> cm <sup>-3</sup>	m
CRAIRC	critical soil air content for aeration	0.075	cm <sup>3</sup> cm <sup>-3</sup>	d

d, default; e, estimated; m, measured; m-c, calibrated on the basis of the measured data; d-c, fine tuning around default data. TDWI = 15.1 kg ha<sup>-1</sup> for 2016, 17.2 kg ha<sup>-1</sup> for 2017, and 19.4 kg ha<sup>-1</sup> for 2018, respectively, with an increase in tree age.

First, corrected values of TSUMEM, TSUM1 and TSUM2 were 230, 967, and 960 °C, respectively (Table 2), which were calculated by the average temperatures and developmental stages from 2016 and 2017. Main weather parameters (average air temperature, AT; average irradiation, AI; and total precipitation, TP) are given in Table 3. Furthermore, the highest average daily radiation amount occurred in 2017, followed by 2018, and finally 2016. During the whole growth season, there was a small deviation in total rainfall for three years, ranging from 72.7 to 96.8 mm. However, in 2018, 64% of precipitation occurred between emergence and flowering, while in 2016 and 2017 most precipitation fell after flowering.

Table 3. Phenological phases and main weather characteristics.

Phase	AT (°C)			AI (MJ m <sup>-2</sup> d <sup>-1</sup> )			TP (mm)		
	2016	2017	2018	2016	2017	2018	2016	2017	2018
Beginning-Emergence	16.4	15.7	15.5	12.4	15.1	11.8	1	6	1
Emergence-flowering	23.9	23.9	23.1	19.8	22.3	20.3	19	15	46
Flowering-maturity	23.2	21.8	23.2	18.1	17.8	18.6	76	61	26
Whole season	23.6	22.9	23.1	18.9	20.1	19.5	97	83	73

AT: daily average air temperature; AI: daily average irradiation; TP: total precipitation; Whole season: the length of from emergence to maturity. Harvested date: 293rd day for the year 2016; 302nd for the year 2017; 301st for the year 2018.

The calibration performance was first evaluated by the simulated results of the phenological development stages, shown in Table 4. Validated results indicated the differences in simulating the lengths of growth duration, emergence, flowering, and maturity date against observations were −1, −2, −3, and −3 days, respectively. The accuracy was the highest in 2016, followed by 2017 and 2018 based on emergence, flowering, and maturity end date. Although the flowering and maturity dates were overestimated in 2017 and underestimated in 2018, with the range of 2 to 4 days, simulating the length from emergence to flowering and from flowering to maturity suggested a small error ranging from 1 to 2 days. In addition, jujube phenology can be expected to be further corrected by

introducing thermal requirements for flowering and maturity, which have been successfully used in winter wheat [44].

**Table 4.** Calibration and validation results for phenological development stage.

Phase	End Day								
	2016 Calibration			2017 Calibration			2018 Validation		
	Ob	Si	Diff	Ob	Si	Dif	Ob	Si	Diff
Beginning–Emergence	117	116	−1	121	121	0	120	118	−2
Emergence–flowering	187	186	−1	190	192	+2	196	193	−3
Flowering–maturity	260	260	0	271	275	+4	267	264	−3
Whole season	143	144	+1	150	154	+4	147	146	−1

Ob: observation; Si: simulation; Diff: difference between simulated and observed values.

Second, crop growth should not only accurately reflect the developmental stage of phenology, but also simulate growth dynamics of biomass in different organs, especially the total above-ground biomass and leaf area index. According to the phenological development stage, WOFOST distributes the biomass produced to different organs [43]. Calibration and validation results for TAGP in the case of full irrigation in 2016, 2017, and 2018, based on calibrated parameters in Table 2, were shown in Figure 2. Simulated TAGP values agreed with measured values, with a calibrated  $R^2$  of 0.963 in 2016 and 0.978 in 2017, and a validated  $R^2$  of 0.967 in 2018. The model also showed great accuracy in simulating TAGP values (calibrated RMSE = 0.851 t ha<sup>−1</sup> for year 2016 and 0.811 t ha<sup>−1</sup> for year 2017, and validated RMSE = 0.915 t ha<sup>−1</sup> for year 2018). The model simulated almost perfectly the final total biomass obtained in 2017 (15.1 t ha<sup>−1</sup>) with a slight overestimation of 1.5%, but overestimated about 8% in 2016 and 2018. The last three observation points in 2018 were overestimated, resulting in a slightly high deviation (18%, 9%, and 8%, respectively). But the values of predicted final total biomass and yield error were acceptable, which were 8% and 2.8%, respectively. In addition, the yield simulated by WOFOST under the full irrigation treatment was 6.53, 8.92, and 7.55 t ha<sup>−1</sup> for 2016, 2017, and 2018, respectively, whereas the measured yield was 6.38, 9.16, and 7.77 t ha<sup>−1</sup>, respectively. The model showed a relatively good performance for predicting final yield.

Within the calibration and validation datasets, the model succeeded in reproducing a time series of LAI variability during the main growth period in these three years, demonstrated by values of the agreement and error metrics ( $R^2 = 0.933$  and RMSE = 0.144 m<sup>2</sup> m<sup>−2</sup> for 2016,  $R^2 = 0.979$  and RMSE = 0.120 m<sup>2</sup> m<sup>−2</sup> for 2017, and  $R^2 = 0.962$  and RMSE = 0.160 m<sup>2</sup> m<sup>−2</sup> for 2018) (Figure 2). Moreover, time trends of the simulated LAI were in agreement with the actual growth parameters of jujube trees. The peak of the LAI occurred during the fruit-filling period, with a maximum simulated value of 1.57, 2.11, and 2.23 m<sup>2</sup> m<sup>−2</sup> for 2016, 2017, and 2018, respectively, and with a maximum measured value of 1.69, 2.16, and 2.31 m<sup>2</sup> m<sup>−2</sup>, respectively. Although the model slightly underestimated the maximum LAI, the total prediction accuracy was well presented.

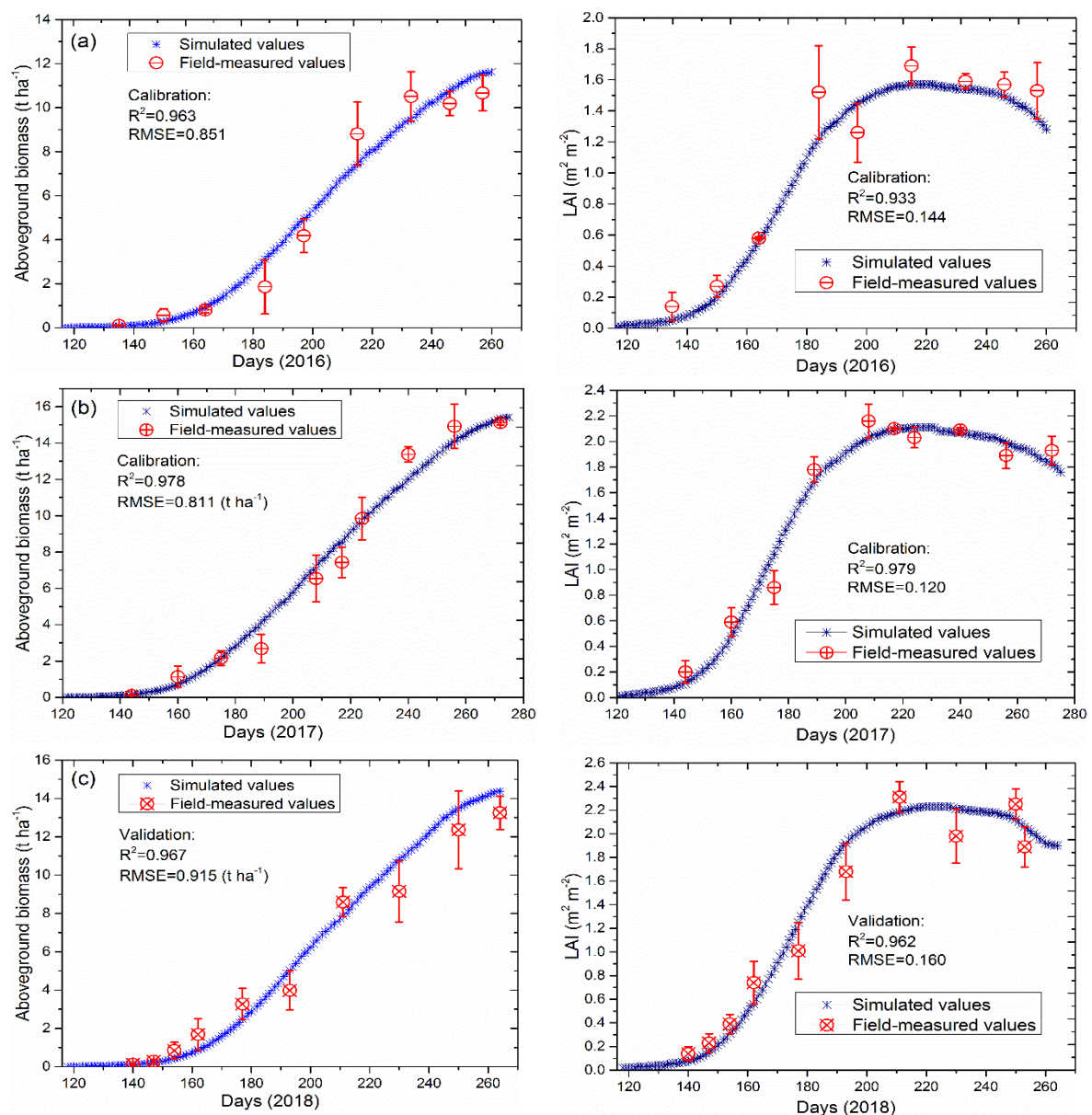


**Figure 2.** Measured and simulated above-ground biomasses and leaf area indices. (a) Year 2016; (b) Year 2017; and (c) Year 2018.

Finally, the WOFOST model accomplished water-limited production by simulating daily soil moisture content, which was the combination of irrigation and rainfall, soil water uptake, soil evaporation, and crop transpiration [45]. Observed and simulated daily soil water content in the case of full irrigation treatment in 2017 are presented in Figure 3, showing  $R^2 = 0.79$  and  $RMSE = 0.01 \text{ cm}^3 \text{ cm}^{-3}$  achieved for all observations. Furthermore,  $R^2$  and RMSE, excluding sample points on the day of irrigation and first day after irrigation, can reach 0.94 and  $0.005 \text{ cm}^3 \text{ cm}^{-3}$ , showing good moisture content simulation performance. The soil moisture content on the day of irrigation and first day after irrigation could not be simulated well, especially the first and second irrigation times, with a maximum deviation of  $0.064$  and  $0.056 \text{ cm}^3 \text{ cm}^{-3}$ , respectively. The reason may be that the drip irrigation was performed at the experimental site so the actual soil moisture content changed slowly. While the WOFOST model employed the original, simple tipping bucket soil water balance approach [18], it may not respond to the effect of irrigation patterns on soil moisture content changes. A multi-layer soil-water-atmosphere-plant (SWAP) parameter can be integrated into the

WOFOST model to successfully model the growth of annual crops and grasslands [46]. However, Rallo et al. [47] compared the performances of SWAP and FAO (Food and Agriculture Organization) Agro-Hydrological models in simulating the soil water contents in a grape garden, with an  $R^2$  of 0.69 and 0.74, RMSE of 0.0209 and 0.0214, respectively, showing slightly lower accuracy than our research results. Eitzinger et al. [40] found that CERES, SWAP, and WOFOST showed almost similar performances in simulating total soil water content of winter wheat and spring barley, ranging from 2.32%–6.77% for wheat and 0.71%–4.67% for barley. Therefore, the performance of different models in simulating the soil moisture content of jujube gardens shall be validated based on a large number of experiments. It may vary with fruit tree variety and soil structure. Another reason may be that, during the emergence phase, less water consumed by jujube transpiration led to high simulation values. Moreover, the mean absolute error (MAE) and the mean bias error (MBE) of simulated soil water content was expressed as  $0.006 \text{ cm}^3 \text{ cm}^{-3}$  and  $0.0006 \text{ cm}^3 \text{ cm}^{-3}$  and was slightly higher than the measured values.

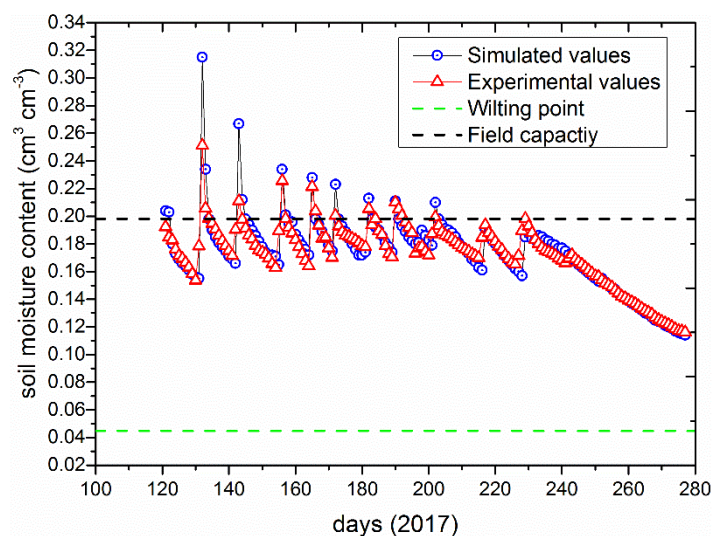


**Figure 3.** Measured and simulated volumetric soil water content values in the whole soil profile. The total soil water content was averaged over the whole soil depth (0–80 cm).

### 3.2. Model Evaluation under Different Irrigation Regimes

The yield data achieved from five irrigation treatments in 2016, 2017, and 2018 (Table 1) were employed to validate the global performance of the model. The model showed a great global accuracy in predicting yield, with good  $R^2 = 0.86$  and  $RMSE = 0.51 \text{ t ha}^{-1}$  values (Figure 4a). In total, 60% of the samples were underestimated. Moreover, the performance was evaluated by plotting the yield prediction error against the total irrigation amount during the main growth period (Figure 4b). There was a reasonable error of  $\pm 0.7 \text{ t ha}^{-1}$  for 14 samples, and 75% of the samples displayed a prediction error of less than  $0.5 \text{ t ha}^{-1}$ , with the exception of the D3 treatment in 2017, which was markedly underestimated with an error of  $1.1 \text{ t ha}^{-1}$ . The mean absolute error (MAE) under D1 treatment expressed a minimum of  $0.2 \text{ t ha}^{-1}$ , followed by D2 and D4 irrigation degrees, and finally D3 and D5.

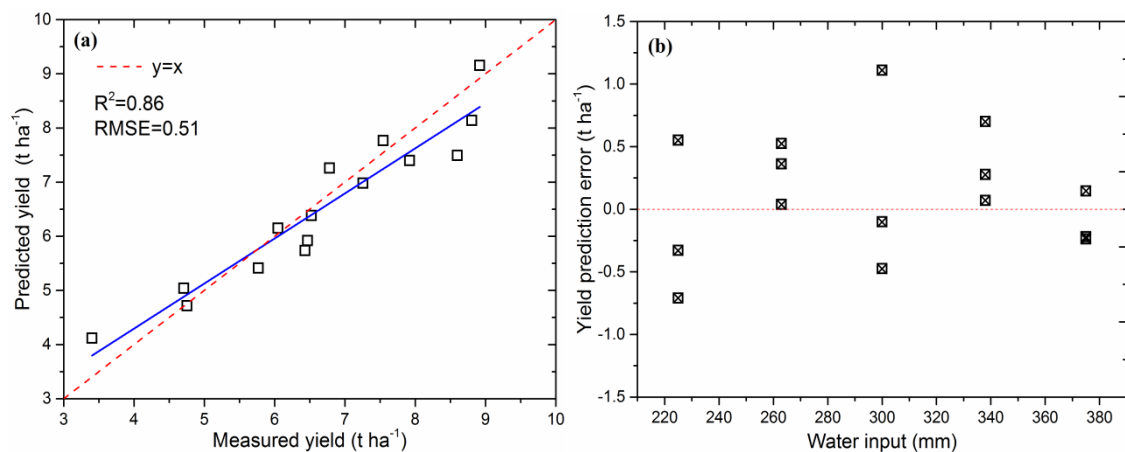


**Figure 4.** (a) Model performance evaluation for global accuracy; (b) Yield prediction error for five irrigation degrees.

Verification results for different growing seasons are shown in Table 5. The comparison of simulated yield against actual yield showed good local agreement for each growth season ( $R^2 \geq 0.8$ ) and prediction accuracy ( $RMSE \leq 0.62 \text{ t ha}^{-1}$ ). MAE ranged from 0.33 to  $0.62 \text{ t ha}^{-1}$ , showing a slightly higher value in 2017. The reason may be that D3 processing in 2017 had a high yield prediction bias, which in turn led to the highest RMSE, MAE, and MBE values.

**Table 5.** Simulation performance for different years.

Year	R <sup>2</sup>	RMSE(t ha <sup>-1</sup> )	MAE(t ha <sup>-1</sup> )	MBE(t ha <sup>-1</sup> )
2016	0.93	0.41	0.34	-0.02
2017	0.80	0.62	0.62	-0.52
2018	0.90	0.31	0.33	+0.08

Simulated days of drought stress under different irrigation treatments increased with the decrease of irrigation amount during each growth season correspondingly (Figure 5). The ratio of water stress days to the length of the growth period in 2017 was lower than 2016 and 2018, ranging from 6% to 41% for D1 to D5 treatments in 2017, 8% to 67% in 2016, and 14% to 43% in 2018. The main reason was that the average temperature in 2017 was lower than 2016 and 2018, which led to a low average evapotranspiration. In addition, during the period from emergence to flowering, the rainfall in 2018 was higher than 2016 and 2017, resulting in a relatively small number of water stress days. Nevertheless, during the stages of flowering to maturity, relatively low rainfalls slightly produced more days of water stress. The model responded well to the effects of temperature and rainfall on the number of days of water stress.

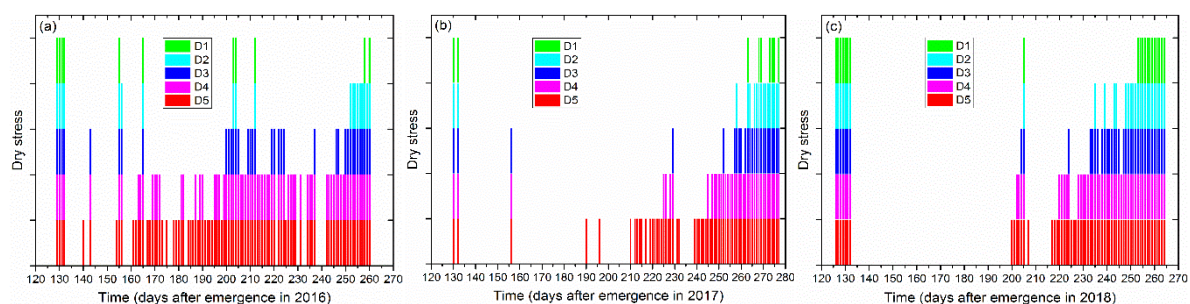


**Figure 5.** Days with dry stress conditions in three years. (a) year 2016; (b) year 2017; and (c) 2018.

The prediction yields slowly declined from D1 to D3, with a range from 1.2% to 10% (Figure 6). For D4 and D5 treatments, reduction ratios ranged from 23% to 47%, except for D4 treatment in 2017 (11.2%). In the case of the same irrigation treatments, the rate of yield decline from 2017 was also significantly lower than the other two years. One reason may be that the spring irrigation volume on the 115th day of 2017 was 50 mm higher than 2016 and 2018, which resulted in a significant decrease in the number of water stress days during the emergence period. Another reason, as mentioned before, may be that the average temperature of flowering to maturity was about 1.4 °C lower in 2017 than in 2016 and 2018, thereby resulting in fewer days of water stress and a long fruit-filling period. The research results also suggested that 80% of full irrigation can be a critical irrigation amount (decline ratio  $\leq 10\%$ ), and 90% of full irrigation might achieve a balance between guaranteed production and water conservation (average decline ratio  $\leq 3.8\%$ ).

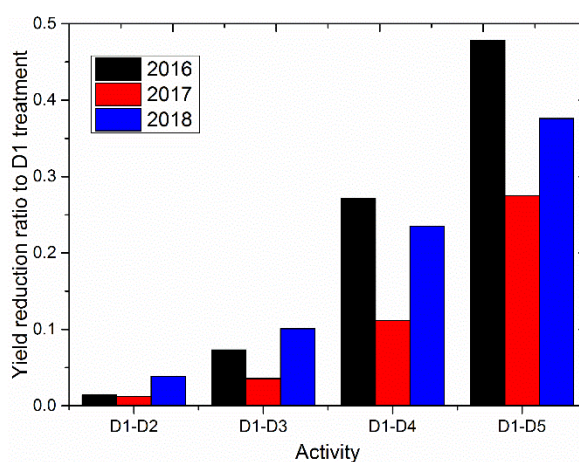


**Figure 6.** The simulation yield decline rate of different irrigation treatments in three years.

In this research, WOFOST was confirmed to hold confidence in estimating water-limited production for jujube fruit trees. Previous research has also proved that the AquaCrop model showed good yield prediction ability for peach trees under water stress [37], with the index of agreement higher than 0.867 and the correlation coefficient higher than 0.825, respectively. Total yield compared with RDI<sub>75</sub> (75% of full irrigation) treatment was decreased by 32%. It was almost in line with our research results—that the yield was significantly reduced when the irrigation volume dropped to 70% of full irrigation. Marsal and Stöckle found that the CropSyst model can be used for scheduling regulated deficit irrigation for pear trees, with a determination coefficient of 0.85 for transpiration [39]. Rallo et al. [38] employed the AQUACROP model to evaluate the transpiration reductions of mature olive trees, showing a correlation coefficient ( $r$ ) of 0.9 and an RMSE of 0.14 between the crop transpiration reduction coefficient ( $K_s$ ) and function of the relative depletion ( $D_{rel}$ ) for predawn leaf water potential (PLWP), and  $r = 0.86$  and RMSE = 0.14 for midday stem water potential (MSWP). Moreover, there may be certain differences in the performance of the models depending on the crop varieties, irrigation systems, and purposes. Todorovic et al. [15] found that the biomass growth simulation for sunflowers by WOFOST was superior to AquaCrop and CropSyst under rain-fed and regulated deficit irrigation. Nevertheless, both AquaCrop and CropSyst performed well under slight-to-moderate water stress conditions. Therefore, the model should be chosen according to crop varieties, irrigation modes, and purposes, and calibrated and validated based on a large number of detailed experimental data.

In order to confirm whether the WOFOST model can scientifically respond to the growth of jujube trees with different irrigation treatments, the same full irrigation amount was adopted in three years, which was also widely used in the local area. Figure 5 also shows that the jujube trees under full irrigation were still under water stress for several days per year. Moreover, there were deviations in the time and number of days under water stress in different years. This also indicated that crop water

requirements were greatly affected by temperature and crop phenology. The full irrigation schedule, by referring to an excel-based irrigation management method [42], is expected to be adjusted and validated by the detailed experiments.

In addition, as mentioned above, the biggest difference between perennial fruit trees and annual crops is the effect of tree age and tree shape on the initial dry weight and canopy structure, which leads to significant deviations of the initial dry weight (TDWI) and CO<sub>2</sub> assimilation parameters of fruit trees in different regions. Considering the leaf area index (LAI) can respond well to these parameters [18], a time series of reliable LAI acquired by remote sensing images could also be used to optimize TDWI and CO<sub>2</sub> assimilation parameters to solve this problem. Then, the model could be expected to be applied to fruit tree growth simulations at the regional scale.

#### 4. Conclusions

Research results showed that the calibrated WOFOST model can reasonably simulate the growth dynamics of TAGP and LAI for jujube fruit trees, as well as soil moisture content. Nevertheless, the model cannot accurately simulate the soil moisture content on the day of irrigation and first day after irrigation, with a relatively high deviation. In addition, the model showed a greater global accuracy in predicting yield under different irrigation treatments, with good R<sup>2</sup> and RMSE values. There was a relatively small deviation for most of the irrigation treatments, with the exception of the 80% treatment of full irrigation in 2017. The ratio of water stress days to the length of growth period in 2017 was lower than 2016 and 2018, which showed a good temperature response. The results also suggested that the water requirement for jujube production should be no less than 80% of full irrigation, and 90% of the full irrigation can be recommended to achieve a balance between production and water savings. Further analysis of soil moisture simulation results at different tree ages or the use of more elaborate experimental data can also be expected to improve the accuracy of the simulation.

**Author Contributions:** T.B. methodology and writing original draft preparation. N.Z. investigation. B.M. and Y.C. review, editing and supervision.

**Funding:** This research was funded by National Natural Science Foundation of China (41561088 and 61501314), Science & Technology Nova Program of Xinjiang Production and Construction Corps (2018CB020), and Tarm University President Fund (2015002).

**Acknowledgments:** The authors would like to thank the editors and anonymous reviewers for valuable comments, which are significant for improving this manuscript.

**Conflicts of Interest:** The authors declare no conflict of interest.

#### References

1. Li, J.W.; Fan, L.P.; Ding, S.D.; Ding, X.L. Nutritional composition of five cultivars of chinese jujube. *Food Chem.* **2007**, *103*, 454–460. [[CrossRef](#)]
2. Zhu, K.Y.; Tsim, K.W.K.; Chen, J.; Lam, C.T.W.; Li, Z.; Maiwulanjiang, M.; Lau, D.T.W.; Zhan, J.Y.X.; Choi, R.C.Y.; Zhang, W.L.; et al. Chemical and Biological Assessment of Ziziphus jujuba Fruits from China: Different Geographical Sources and Developmental Stages. *J. Agric. Food Chem.* **2013**, *61*, 7315–7324.
3. Ewert, F.; Rötter, R.P.; Bindi, M.; Webber, H.; Trnka, M.; Kersebaum, K.C.; Olesen, J.E.; van Ittersum, M.K.; Janssen, S.; Rivington, M.; et al. Crop modelling for integrated assessment of risk to food production from climate change. *Environ. Model. Softw.* **2015**, *72*, 287–303. [[CrossRef](#)]
4. Supit, I.; van Diepen, C.A.; De Wit, A.J.W.; Wolf, J.; Kabat, P.; Baruth, B.; Ludwig, F. Assessing climate change effects on European crop yields using the Crop Growth Monitoring System and a weather generator. *Agric. For. Meteorol.* **2012**, *164*, 96–111. [[CrossRef](#)]
5. Van Walsum, P.E.V.; Supit, I. Influence of ecohydrologic feedbacks from simulated crop growth on integrated regional hydrologic simulations under climate scenarios. *Hydrol. Earth Syst. Sci.* **2012**, *16*, 1577–1593. [[CrossRef](#)]

6. Kroes, J.G.; Supit, I. Impact analysis of drought, water excess and salinity on grass production in The Netherlands using historical and future climate data. *Agric. Ecosyst. Environ.* **2011**, *144*, 370–381. [[CrossRef](#)]
7. Supit, I.; van Diepen, C.A.; de Wit, A.J.W.; Kabat, P.; Baruth, B.; Ludwig, F. Recent changes in the climatic yield potential of various crops in Europe. *Agric. Syst.* **2010**, *103*, 683–694. [[CrossRef](#)]
8. Alexandrov, V.A.; Eitzinger, J.J. The Potential Effect of Climate Change and Elevated Air Carbon Dioxide on Agricultural Crop Production in Central and Southeastern Europe. *J. Crop Improv.* **2005**, *13*, 291–331. [[CrossRef](#)]
9. Palosuo, T.; Kersebaum, K.C.; Angulo, C.; Hlavinka, P.; Moriondo, M.; Olesen, J.E.; Patil, R.H.; Ruget, F.; Rumbaur, C.; Takáč, J.; et al. Simulation of winter wheat yield and its variability in different climates of Europe: A comparison of eight crop growth models. *Eur. J. Agron.* **2011**, *35*, 103–114. [[CrossRef](#)]
10. De Wit, A.; Baruth, B.; Boogaard, H.; Van Diepen, K.; Van Kraalingen, D.; Micale, F.; Te Roller, J.; Supit, I.; Van Den Wijngaart, R. Using ERA-INTERIM for regional crop yield forecasting in Europe. *Clim. Res.* **2010**, *44*, 41–53. [[CrossRef](#)]
11. De Wit, A.J.W.; van Diepen, C.A. Crop growth modelling and crop yield forecasting using satellite-derived meteorological inputs. *Int. J. Appl. Earth Obs. Geoinf.* **2008**, *10*, 414–425. [[CrossRef](#)]
12. Dobermann, A.; Dawe, D.; Roetter, R.P.; Cassman, K.G. Reversal of rice yield decline in a long-term continuous cropping experiment. *Agron. J.* **2000**, *92*, 633–643. [[CrossRef](#)]
13. Bussay, A.; van der Velde, M.; Fumagalli, D.; Seguni, L. Improving operational maize yield forecasting in Hungary. *Agric. Syst.* **2015**, *141*, 94–106. [[CrossRef](#)]
14. Asseng, S.; Ewert, F.; Rosenzweig, C.; Jones, J.W.; Hatfield, J.L.; Ruane, A.C.; Boote, K.J.; Thorburn, P.J.; Rötter, R.P.; Cammarano, D.; et al. Uncertainty in simulating wheat yields under climate change. *Nat. Clim. Chang.* **2013**, *3*, 827–832. [[CrossRef](#)]
15. Todorovic, M.; Albrizio, R.; Zivotic, L.; Abi Saab, M.T.; Stöckle, C.; Steduto, P. Assessment of aquacrop, cropsyst, and WOFOST models in the simulation of sunflower growth under different water regimes. *Agron. J.* **2009**, *101*, 509–521. [[CrossRef](#)]
16. Confalonieri, R.; Acutis, M.; Bellocchi, G.; Donatelli, M. Multi-metric evaluation of the models WARM, CropSyst, and WOFOST for rice. *Ecol. Modell.* **2009**, *220*, 1395–1410. [[CrossRef](#)]
17. De Wit, A.; Boogaard, H.; Fumagalli, D.; Janssen, S.; Knapen, R.; van Kraalingen, D.; Supit, I.; van der Wijngaart, R.; van Diepen, K. 25 years of the WOFOST cropping systems model. *Agric. Syst.* **2019**, *168*, 154–167. [[CrossRef](#)]
18. Van Diepen, C.A.; Wolf, J.; van Keulen, H.; Rappoldt, C. WOFOST: A simulation model of crop production. *Soil Use Manag.* **1989**, *5*, 16–24. [[CrossRef](#)]
19. Jones, J.W.; Hoogenboom, G.; Porter, C.H.; Boote, K.J.; Batchelor, W.D.; Hunt, L.A.; Wilkens, P.W.; Singh, U.; Gijsman, A.J.; Ritchie, J.T. The DSSAT cropping system model. *Proc. Eur. J. Agron.* **2003**, *18*, 235–265. [[CrossRef](#)]
20. Wang, X.; Williams, J.R.; Gassman, P.W.; Baffaut, C.; Izaurralde, R.C.; Jeong, J.; Kiniry, J.R. EPIC and APEX: Model Use, Calibration, and Validation. *Trans. Asabe.* **2012**, *55*, 1447–1462. [[CrossRef](#)]
21. Brisson, N.; Gary, C.; Justes, E.; Roche, R.; Mary, B.; Ripoche, D.; Zimmer, D.; Sierra, J.; Bertuzzi, P.; Burger, P.; et al. An overview of the crop model STICS. *Proc. Eur. J. Agron.* **2003**, *18*, 309–332. [[CrossRef](#)]
22. Holzworth, D.P.; Huth, N.I.; deVoil, P.G.; Zurcher, E.J.; Herrmann, N.I.; McLean, G.; Chenu, K.; van Oosterom, E.J.; Snow, V.; Murphy, C.; et al. APSIM—Evolution towards a new generation of agricultural systems simulation. *Environ. Model. Softw.* **2014**, *62*, 327–350. [[CrossRef](#)]
23. Van Dam, J.C.; Wesseling, J.G.; Feddes, R.A.; Kabat, P.; Van Walsum, P.E.V.; Diepen, C.A. Van Theory of SWAP version 2.0. *Softw. Man.* **1997**, *153*.
24. Raes, D.; Steduto, P.; Hsiao, T.C.; Fereres, E. Aquacrop—The FAO crop model to simulate yield response to water: II. main algorithms and software description. *Agron. J.* **2009**, *101*, 438–447. [[CrossRef](#)]
25. Stöckle, C.O.; Donatelli, M.; Nelson, R. CropSyst, a cropping systems simulation model. *Proc. Eur. J. Agron.* **2003**, *18*, 289–307. [[CrossRef](#)]
26. Abedinpour, M.; Sarangi, A.; Rajput, T.B.S.; Singh, M.; Pathak, H.; Ahmad, T. Performance evaluation of AquaCrop model for maize crop in a semi-arid environment. *Agric. Water Manag.* **2012**, *110*, 55–66. [[CrossRef](#)]

27. Aggarwal, P.K.; Banerjee, B.; Daryaei, M.G.; Bhatia, A.; Bala, A.; Rani, S.; Chander, S.; Pathak, H.; Kalra, N. InfoCrop: A dynamic simulation model for the assessment of crop yields, losses due to pests, and environmental impact of agro-ecosystems in tropical environments. II. Performance of the model. *Agric. Syst.* **2006**, *89*, 47–67. [[CrossRef](#)]
28. Bregaglio, S.; Frasso, N.; Pagani, V.; Stella, T.; Francone, C.; Cappelli, G.; Acutis, M.; Balaghi, R.; Ouabbou, H.; Paleari, L.; et al. New multi-model approach gives good estimations of wheat yield under semi-arid climate in Morocco. *Agron. Sustain. Dev.* **2014**, *35*, 157–167. [[CrossRef](#)]
29. Chen, C.; Wang, E.; Yu, Q. Modelling the effects of climate variability and water management on crop water productivity and water balance in the North China Plain. *Agric. Water Manag.* **2010**, *97*, 1175–1184. [[CrossRef](#)]
30. Eweys, O.A.; Elwan, A.A.; Borham, T.I. Integrating WOFOST and Noah LSM for modeling maize production and soil moisture with sensitivity analysis, in the east of The Netherlands. *F. Crop. Res.* **2017**, *210*, 147–161. [[CrossRef](#)]
31. García-Vila, M.; Fereres, E. Combining the simulation crop model AquaCrop with an economic model for the optimization of irrigation management at farm level. *Eur. J. Agron.* **2012**, *36*, 21–31. [[CrossRef](#)]
32. Geerts, S.; Raes, D.; Garcia, M. Using AquaCrop to derive deficit irrigation schedules. *Agric. Water Manag.* **2010**, *98*, 213–216. [[CrossRef](#)]
33. Kroes, J.G. Modeling water management strategies using the SWAP/WOFOST model. In Proceedings of the Climate Variability, Modeling Tools and Agricultural Decision-Making. In Proceedings of the AGRIDEMA Workshop, Valladolid, Spain, 28–29 June 2007; pp. 127–136.
34. McNider, R.T.; Handyside, C.; Doty, K.; Ellenburg, W.L.; Cruise, J.F.; Christy, J.R.; Moss, D.; Sharda, V.; Hoogenboom, G.; Caldwell, P. An integrated crop and hydrologic modeling system to estimate hydrologic impacts of crop irrigation demands. *Environ. Model. Softw.* **2015**, *72*, 341–355. [[CrossRef](#)]
35. Zhou, J.; Cheng, G.; Li, X.; Hu, B.X.; Wang, G. Numerical Modeling of Wheat Irrigation using Coupled HYDRUS and WOFOST Models. *Soil Sci. Soc. Am. J.* **2012**, *76*, 648. [[CrossRef](#)]
36. Qin, W.; Heinen, M.; Assinck, F.B.T.; Oenema, O. Exploring optimal fertigation strategies for orange production, using soil-crop modelling. *Agric. Ecosyst. Environ.* **2016**, *223*, 31–40. [[CrossRef](#)]
37. Ismail, S.M.; El-Abedin, T.K.Z.; El-Ansary, D.O.; El-Al, A.A. Modification of FAO Crop Model to Simulate Yield Response to Water for Peach Trees. *Irrig. Drainage.* **2015**, *32*, 145–172.
38. Rallo, G.; Agnese, C.; Minacapilli, M.; Provenzano, G. Assessing AQUACROP water stress function to evaluate the transpiration reductions of olive mature tree. *Ital. J. Agrometeorol.* **2012**, *1*, 21–28.
39. Marsal, J.; Stöckle, C.O. Use of CropSyst as a decision support system for scheduling regulated deficit irrigation in a pear orchard. *Irrig. Sci.* **2012**, *30*, 139–147. [[CrossRef](#)]
40. Eitzinger, J.; Trnka, M.; Hösch, J.; Žalud, Z.; Dubrovský, M. Comparison of CERES, WOFOST and SWAP models in simulating soil water content during growing season under different soil conditions. *Ecol. Modell.* **2004**, *171*, 223–246. [[CrossRef](#)]
41. Abi Saab, M.T.; Todorovic, M.; Albrizio, R. Comparing aquaCrop and cropSyst models in simulating barley growth and yield under different water and nitrogen regimes: Does calibration year influence the performance of crop growth models? *Agric. Water Manag.* **2015**, *147*, 21–33. [[CrossRef](#)]
42. Todorovic, M. An excel-Based tool Forreal-Time irrigation management at field scale. In Proceedings of the International Symposium on Water and Land Management for Sustainable Irrigated Agriculture, Adana, Turkey, 4–8 April 2006.
43. De Wit, A.; Wolf, J. *Calibration of WOFOST Crop Growth Simulation Model for Use within CGMS*; Plant Production Systems Group, Wageningen University: Wageningen, Holland, 2010; pp. 1–38.
44. Ceglar, A.; van der Wijngaart, R.; de Wit, A.; Lecerc, R.; Boogaard, H.; Seguini, L.; van den Berg, M.; Toreti, A.; Zampieri, M.; Fumagalli, D.; et al. Improving WOFOST model to simulate winter wheat phenology in Europe: Evaluation and effects on yield. *Agric. Syst.* **2019**, *168*, 168–180. [[CrossRef](#)]
45. Joint Research Centre (European Commission). *An Agricultural Information System System Description of the Wofost 6. 0 Crop Simulation Model Implemented in Cgms Volume 1: Theory and Algorithms*; European Commission: Luxembourg, 1994.

46. Kroes, J.G.; Van Dam, J.C.; Groenendijk, P.; Hendriks, R.F.A.; Jacobs, C.M.J. *SWAP Version 4.0: Theory Description and User Manual*; Wageningen UR-Wageningen Environmental Research: Wageningen, Holland, 2017.
47. Rallo, G.; Agnese, C.; Minacapilli, M.; Provenzano, G. Comparison of SWAP and FAO Agro-Hydrological Models to Schedule Irrigation of Wine Grapes. *J. Irrig. Drain. Eng.* **2011**, *138*, 581–591. [[CrossRef](#)]



© 2019 by the authors. Licensee MDPI, Basel, Switzerland. This article is an open access article distributed under the terms and conditions of the Creative Commons Attribution (CC BY) license (<http://creativecommons.org/licenses/by/4.0/>).